LABORATORY SCIENCE

Effect of intraocular lens decentration on image quality tested in a custom model eye

Pablo Pérez-Merino, PhD, Susana Marcos, PhD

Purpose: To evaluate the effect of intraocular lens (IOL) decentration on optical aberrations with different IOL designs.

Setting: Visual Optics and Biophotonics Laboratory, Instituto de Óptica, Consejo Superior de Investigaciones Científicas, Madrid, Spain.

Design: Experimental study.

Methods: The following 18 aspheric IOLs immersed in a physical model eye were measured using a laser ray-tracing aberrometer: 10 Vivinex XY1 with spherical aberration correction of −0.18 μm (V-0.18), 4 Tecnis 1P ZCB00V with spherical aberration correction of −0.27 μm (T-0.27), and 4 Acrysof 1P SN60WF with spherical aberration correction of −0.17 μm (A-0.17). The optical aberrations were evaluated with the IOL on axis and 0.4 mm and 0.7 mm laterally decentered. The laser ray tracing–measured aberrations were compared with aberrations estimated using virtual ray tracing. Retinal image quality was evaluated from the modulation transfer function (MTF) and visual Strehl ratio.

Results: Wave aberration measurements of the same IOL were highly repetitive (deviation <0.02 μm). Astigmatism and coma increased with decentration at a rate of 0.18 μm/mm and 0.19 μm/mm for the V-0.18, 0.20 μm/mm and 0.32 μm/mm for the T-0.27, and 0.26 μm/mm and 0.39 μm/mm for the A-0.17, respectively. The 0.7 mm lateral decentration decreased the visual Strehl ratio by 2.23 times for the V-0.18, by 2.8 times for the T-0.27, and by 3.2 times for the A-0.17. The V-0.18 showed the highest MTF and visual Strehl values for all centration values.

Conclusions: Lateral decentration resulted in decreased retinal image quality. The V-0.18 was the most immune design to optical degradation caused by decentration.

J Cataract Refract Surg 2018; 44:889–896 © 2018 ASCRS and ESCRS

Supplemental material available at www.jcrsjournal.org.

Standard cataract surgery has evolved over the years, including the introduction of intraocular lenses (IOLs) with new optical designs. In general, state-of-the-art monofocal IOLs have aspheric surfaces with the aim at reducing the positive spherical aberration of the cornea, mimicking the spherical aberration balance between the cornea and crystalline lens in the young eye, thereby improving retinal image quality.[1–4] Increasing the number of IOL surface design parameters allows better control for reducing higher-order aberrations (HOAs) (eg, astigmatism or coma)[5] and improving optical quality both on-axis and off-axis.[6]

As IOL designs become more complex, the final position of the IOL is more critical.[1,7–9] Studies[8,10,11] show that the image quality of traditional aspheric IOLs with negative spherical aberration decreases with IOL misalignment, declining to levels below that of a spherical IOL at approximately 0.5 mm. Notably, this is the range (0.2 to 0.5 mm) of mean IOL misalignment.[8,11,12] Misalignment of the implanted IOL has been associated with numerous factors, including a large capsulorhexis, capsule fibrosis, an asymmetric capsule, IOL diameter versus bag diameter, IOL placement in the sulcus, or haptic design, all of which are related to a significant decrease in image quality.[13] On the other hand, the natural misalignment of the capsular bag is usually preserved in uneventful cataract surgery.[14] Calculations using custom eye models show that the presence of some misalignment improved optical quality over no tilt or

Submitted: February 23, 2017 | Final revision submitted: February 8, 2018 | Accepted: February 11, 2018

From Visual Optics and Biophotonics Laboratory, Instituto de Óptica, Consejo Superior de Investigaciones Científicas (IO-CSIC), Madrid, Spain.

Supported in part by a research collaborative project with Hoya Surgical Optics, Inc. This research has received funding from the European Research Council (ERC) under the European Union's Seventh Framework Program (FP/2007-2013)/ERC Grant Agreement (ERC-2011-AdC- 294099) and the Spanish Government FIS2014-56643-R and FIS2017-84753-R to SM.

Corresponding author: Pablo Pérez-Merino, PhD, Visual Optics and Biophotonics Laboratory, Instituto de Óptica Daza de Valdés, Consejo Superior de Investigaciones Científicas, C/Serrano, 121, Madrid 28006, Spain. Email: p.perez@io.cfmac.csic.es.

0886-3350/$ - see frontmatter
https://doi.org/10.1016/j.jcrs.2018.02.025

decentration.[2,8,15] As with the natural lens and unlike spherical IOLs,[16] aspheric IOLs with negative spherical aberration compensate, at least in part, for corneal lateral coma of the opposite sign as a result of geometric passive compensation. Thus, it seems advisable to modulate the design parameters of IOLs to make them less susceptible to potential degradation caused by decentration.

In this study, we evaluated the effect of decentration on the following 3 IOL aspheric designs: the Acrysof 1P SN60WF (Alcon Laboratories, Inc.) with a spherical aberration correction of −0.17 μm (defined in this paper as A-0.17), the Tecnis 1P ZCB00V (Johnson & Johnson Vision Care, Inc.) with aspheric design for spherical aberration correction of −0.27 μm (defined in this paper as T-0.27), and the Vivinex XY1 (Hoya Surgical Optics, Inc.) with new wide-field aspheric optic design for spherical aberration correction of −0.18 μm (defined in this paper as V-0.18). All 3 IOLs are foldable single-piece acrylic. The amount of negative spherical aberration and the mode of action to reduce aberrations are different for the test aspheric IOLs. The A-0.17 IOL, with a posterior aspheric surface, is designed to compensate for 0.17 μm of spherical aberration. It aims to reduce the amount of spherical aberration to approximately 0.1 μm in the pseudophakic eye to mimic that of a natural young phakic eye. The T-0.27 IOL, with an anterior aspheric surface, is designed to compensate for 0.27 μm of spherical aberration, with the aim of eliminating all corneal spherical aberration. The V-0.18 IOL compensates for a spherical aberration of 0.18 μm, similar to the A-0.17 IOL. In addition, the V-0.18 IOL has a second mode of action to eliminate coma, another important aberration. It balances the negative visual effect of coma caused by IOL misalignment in the pseudophakic eye. It does this by modulating optical surfaces using a technology designed to balance the coma aberration (U.S. patent US 8,647,383 B2[17]).

The impact of IOL decentration was evaluated using physical wet-cell eye models, mimicking anatomic parameters of the pseudophakic eye (with artificial aspheric corneas and interocular distances). The use of physical eye models allows experimental testing of factors that might influence optical image quality and its degradation with IOL decentration, including the manufacturing variations of commercially available IOLs.[18] Previous studies[2,11] evaluated the effect of IOL decentration using computer simulations in computer model eyes, typically assuming ideal conditions based on nominal geometry. On the other hand, studies of the measurement of IOL misalignment in patients in vivo (using Purkinje imaging and Scheimpflug imaging[10,19] or optical coherence tomography [OCT][14,20]) evaluated the effect of the specific measured IOL tilt and decentration on image quality and compared it with the effect of a perfectly aligned IOL. These studies were limited to a given IOL model per eye.

Therefore, a better understanding of the impact of IOL decentration on optical quality and its dependence on IOL design will help surgeons select the most suitable IOL for an individual patient. It will also contribute to the improvement of IOL designs.

MATERIAL AND METHODS

Physical Model Eye

A physical model eye was designed for this study. It consisted of an artificial cornea, an IOL holder with a micron rotational-translational stage, and an artificial retina immersed in a balanced salt solution. The balanced salt solution container, the IOL holder, and the artificial retina were built on a 3-dimension printer in acrylonitrile butadiene styrene material. The container was designed with a circular window (12.0 mm diameter) on which the artificial cornea is attached. The IOL holder was designed with a circular window (6.0 mm diameter). The IOL haptics were carefully fixed to the IOL holder with adhesive tape through a surgical microscope (Opmi Pico Zeiss, Carl Zeiss Meditec AG). Intraocular lens decentration in the horizontal direction was achieved by moving the micron rotational-translational stage (within 10 μm of accuracy).

Three aspheric corneas were built using enflufocon A (Boston ES, Bausch & Lomb) and designed with different magnitudes of spherical aberration (Conóptica, S.L.).

Eighteen aspheric IOL samples (IOL power 21.0 diopters [D]) from 3 companies were evaluated as follows: 10 IOLs, V-0.18; 4 IOLs, T-0.27; and 4 IOLs, A-0.17. All IOL models were monofocal acrylic and aspheric with a 6.0 mm optic diameter; however, they differed in their optical design.

Noncontact Profilometry

The geometry of the 3 aspheric corneas and all IOLs was characterized using microscopy-based noncontact profilometry (PLu2300, Sensofar Corp.). The nominal precision on rigid samples was 0.1 μm. Repeated measurements of the corneal and IOL surfaces were taken in a 10.0 mm and 6.0 mm diameter area (centered in apical position), respectively.

Optical Coherence Tomography: Eye Model Alignment

A custom spectral OCT instrument previously described in detail[14,20] was used to quantify interocular distances and IOL centration. Briefly, the setup was based on a fiber optics Michelson interferometer configuration with a superluminescent diode (λ_0 = 840 nm and $\Delta\lambda$ = 50 nm, with λ_0 being center wavelength and $\Delta\lambda$ being bandwidth wavelength) as a light source and a spectrometer consisting of a volume-diffraction grating and complementary metal-oxide semiconductor camera as a detector. The theoretical axial resolution was 3.4 μm in air. Measurements were collected in 10.0 mm × 10.0 mm area and consisted of a collection of 100 B-scans, each composed of 1000 A-scans. The specular reflection of the corneal and IOL surfaces was used to ensure accurate alignment and lateral displacement.

Laser Ray Tracing: Total Wave Aberration Measurements

Total wave aberrations were measured with the IOL centered in the artificial eye (cornea and IOL centered in optical axis) and at 2 horizontal decentrations (0.4 mm and 0.7 mm) using a custom laser ray-tracing aberrometer, which has been described in detail.[21]

The literature reports an average decentration of approximately 0.3 mm,[10,19] with relatively large (up to 0.39 mm) standard deviations (SDs) across patients. Therefore, the studied decentrations cover reported ranges in the literature; for example, Tandogan et al.[22] analyzed optical performance with decentration (up to 1.0 mm).

The sampling pattern of the laser ray tracing was adjusted to fit a 4.0 mm pupil diameter in the custom physical eye model. An infrared (785 nm) laser beam sequentially sampled 37 pupil positions in a hexagonal pattern in 1.5 seconds. Ray aberrations were

obtained by estimating the deviations of the centroids of the retinal spots images corresponding to each entry pupil position with respect to the reference (chief ray). Each IOL sample was measured with each of the 3 corneas (with different anterior surface asphericity) and with 3 magnitudes of decentration (0.0 mm, 0.4 mm, and 0.7 mm). Each set of measurements consisted of 3 runs for every magnitude of decentration, and the results presented are the average of the corresponding 3 repeated measurements. This provided 486 measurements. Figure S1 (available at http://jcrsjournal.org) shows the OCT and laser ray-tracing illustration of the physical eye model.

Virtual Ray Tracing on Custom Model Eye

Total wave aberrations were estimated from ray-tracing analysis on the OCT-based axial distances and profilometry-based corneal and IOL surface geometry. The cornea and IOL surfaces were exported to Zemax Focus software (Radiant Vision Systems). Matlab software (Mathworks, Inc.) was used to create a file suitable to be input into the Zemax dynamic data exchange toolbox.[23] Corneal refractive index was 1.443 and aqueous-vitreous refractive index was 1.3346. Nominal Abbe numbers and refractive indices were used for the IOL materials[24] for the T-0.27 and A-0.17 materials, respectively. Wave aberrations were calculated by tracing an array of 64 × 64 collimated infrared light beams (785 nm, same as laser ray tracing) within a 4.0 mm pupil diameter area through the 4 surfaces (cornea and IOL).

Optical Quality Metrics

Wave aberrations were described in terms of individual Zernike coefficients or the root mean square (RMS). The RMS was used to report the magnitude of HOAs and certain relevant aberrations. The point-spread function (PSF), the modulation transfer function (MTF), and the visual Strehl ratio were computed using Fourier optics routines written in Matlab.

The impact of chromatic defocus on image quality (to capture polychromatic effects that would occur in the real world) was analyzed in terms of the drop in visual Strehl values at best focus for green (555 nm) and at the computed chromatic difference of focus for red (680 nm) using Abbe numbers and refractive indices for the lens materials. Based on experimental data in pseudophakic eyes,[21,24,25] no change in HOAs with wavelength was considered.

Statistical Analysis

The changes in the magnitude of decentration and the differences between IOL models were analyzed statistically using an analysis of variance (ANOVA) general linear model for repeated measurements. Significant levels (ANOVA and pair-wise 2-tailed comparison *t* test) were set at a *P* value less than 0.05.

RESULTS

Cornea and Intraocular Lens Geometry (Noncontact Profilometry)

Figure S2 (available at http://jcrsjournal.org) shows the elevation maps of the anterior aspheric surface of the 3 corneas relative to the best-fit sphere (BFS). Table 1 shows individual data of the anterior and posterior surfaces and the corresponding thickness of the artificial cornea.

Figure S1, *B* (available at http://jcrsjournal.org) shows an example of individual elevation maps (relative to the BFS) of the anterior and posterior IOL surfaces for each of the 3 IOL groups based on Zernike fitting for a 4.0 mm diameter and considering the rotationally symmetric Zernike coefficients.

Table 1. Geometric properties of the aspheric corneas. Fitting and the calculation of the corresponding spherical aberration were performed for a 6.0 mm pupil.

Parameter	Cornea 1	Cornea 2	Cornea 3
R (sphere)			
Anterior cornea	7.7614	7.7474	7.809
Posterior cornea	6.4	6.4	6.4
R (conic)			
Anterior cornea	7.6873	7.7061	7.7873
Posterior cornea	—	—	—
Q value			
Anterior cornea	−0.2578	−0.1432	−0.0792
Posterior cornea	—	—	—
Corneal thickness (mm)	0.503	0.501	0.498
Refractive index (n)	1.443	1.443	1.443
SA (μm)	+0.0901	+0.2077	+0.2601

conic = conic fitting (radius and asphericity); Q = asphericity; R = radius (best-fit sphere); SA = spherical aberration

Experimental (Laser Ray Tracing) Versus Simulation Wavefront Aberrations

(Figure S3, *A* (available at http://jcrsjournal.org) compares the experimental wavefront aberrations (laser ray tracing) and simulated wavefront aberrations of 2 IOLs (V-0.18 and A-0.17) for a 4.0 mm pupil. The agreement between laser ray tracing and simulation was good for both IOL models. The mean differences between the laser ray-tracing measurement and the simulation measurement were less than 0.15 μm (astigmatism) and −0.06 μm (coma) with the V-0.18 IOL and less than 0.1 μm (astigmatism) to 0.06 μm (coma) for the A-0.17 IOL. Bland-Altman plots showed agreement between the experimental (laser ray tracing) and simulated measurements for astigmatism and coma in all IOLs for 0.4 mm and 0.7 mm lateral decentrations (Figure S3, *B*, available at http://jcrsjournal.org).

Laser Ray Tracing Wavefront Aberration: Effect of Intraocular Lens Decentration

Figure S4 (available at http://jcrsjournal.org) shows the wavefront maps in the on-axis position and with a horizontal decentration of 0.7 mm (excluding tilt and defocus) for 1 representative IOL sample of each model with all corneas. Repeated wave aberrations measurements were highly reproducible in each IOL for all lateral displacements. The RMS SD for HOAs for repeated measurements was 0.05 μm (average across all IOL samples and decentrations). The RMS SD (astigmatism and coma) in each IOL group was (1) V-0.18: 0.01 μm – astigmatism/0.03 μm – coma (on axis) and 0.03 μm – astigmatism/0.06 μm – coma (0.7 mm decentration); (2) T-0.27: 0.03 μm – astigmatism/0.06 μm – coma (on axis) and 0.05 μm – astigmatism/0.06 μm – coma (0.7 mm decentration); (3) A-0.17: 0.02 μm – astigmatism/0.04 μm – coma (on axis) and 0.04 μm – astigmatism/0.05 μm – coma (0.7 mm decentration).

As expected, the spherical aberration depended on corneal asphericity and, to a lesser extent, on the final adjustment of retinal focus (Figure S5, available at

http://jcrsjournal.org). With cornea 3 (Figure S5, *b*), the V-0.18 IOL showed slightly positive spherical aberration (mean + 0.02 ± 0.02 µm) whereas the T-0.27 IOL and A-0.17 IOL showed negative to nearly zero spherical aberration values (mean −0.02 ± 0.01 µm and −0.01 ± 0.01 µm, respectively).

The following results in this section refer to measurements using cornea 3, very close to the average spherical aberration value of normal human corneas (Z[4,0] = 0.28 µm; 6.0 mm pupil diameter). Figure S6 (available at http://jcrsjournal.org) shows the mean Zernike coefficients (excluding tilt and defocus) in each IOL group. Although most Zernike coefficients did not change significantly with decentration, horizontal decentration led to a significant increase in the magnitude of horizontal/vertical astigmatism Z(2,2) and horizontal coma Z(3,1) in all IOLs ($P < .05$). The magnitude of the change depended on the IOL model.

Figure 1, *A*, shows the RMS astigmatism as a function of decentration for all IOL samples. Figure 1, *B*, shows the mean data and the rate of astigmatism change with decentration, respectively. The decentration increased astigmatism by a mean of 10.4% (0.4 mm) and 16.1% (0.7 mm) in the V-0.18 IOL, 9.7% (0.4 mm) and 16.6% (0.7 mm) in the T-0.27 IOL, and 10.6% (0.4 mm) and 20.4% (0.7 mm) in the A-0.17 IOL.

Figure 2, *A*, shows RMS coma as a function of decentration for all IOL samples. Figure 2, *B*, shows the mean data and the rate of coma change with decentration, respectively. Decentration increased coma by a mean of 10.3% (0.4 mm) and 12.8% (0.7 mm) in the V-0.18 IOL; by 17.9% (0.4 mm) and 25.1% (0.7 mm) in the T-0.27 IOL; and by 22.2% (0.4 mm) and 29.9% (0.7 mm) in the A-0.17 IOL.

To compare the results with equal sample sizes, the computation was repeated by randomly selecting 4 V-0.18 IOLs and repeating the random pick 4 times (Table 2). The statistical comparison with the other 2 groups remained practically unchanged.

Effect of Intraocular Lens Decentration on Retinal Image Quality

Figure 3, *A*, shows the impact of the measured IOL decentration on optical aberrations was analyzed in terms of the MTF and visual Strehl values. It shows the MTF radial profile (including astigmatism and HOAs) for a centered IOL (*A*) and an IOL decentered by 0.4 mm and 0.7 mm (*B*). Lateral decentration led to a decrease in the MTF in all IOL groups; however, the MTF curves varied across the groups. The performance of the V-0.18 IOL was the least affected by decentration.

Figure 3, *B*, shows the corresponding visual Strehl ratio (including astigmatism and HOAs) as a function of IOL decentration. Intraocular lens decentration of 0.7 mm resulted in a decrease in the visual Strehl ratio by 2.23 times (V-0.18), 2.80 times (T-0.27), and 3.2 times (A-0.17). The V-0.18 IOL had the highest absolute optical quality for a centered IOL and at all decentration levels.

Effect of Chromatic Defocus on Retinal Image Quality

The chromatic difference of focus was 1.57 D, 1.09 D, and 1.63 D (blue–red light, 450 to 680 nm) and 0.59 D, 0.43 D, and 0.59 D (green–red light, 550 to 680 nm, for which the

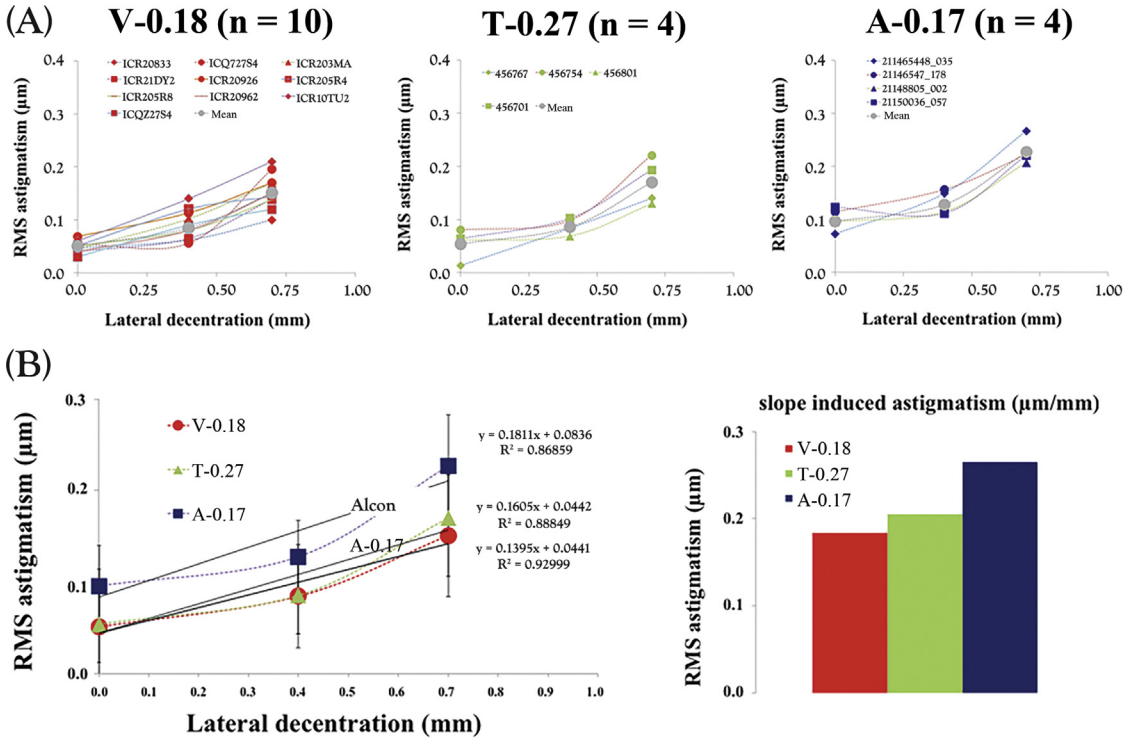

Figure 1. *A*: Root-mean-square astigmatism versus decentration by intraocular lens model. *B*: Root-mean-square astigmatism versus decentration (mean). Data are for a 4.0 mm pupil diameter (RMS = root mean square).

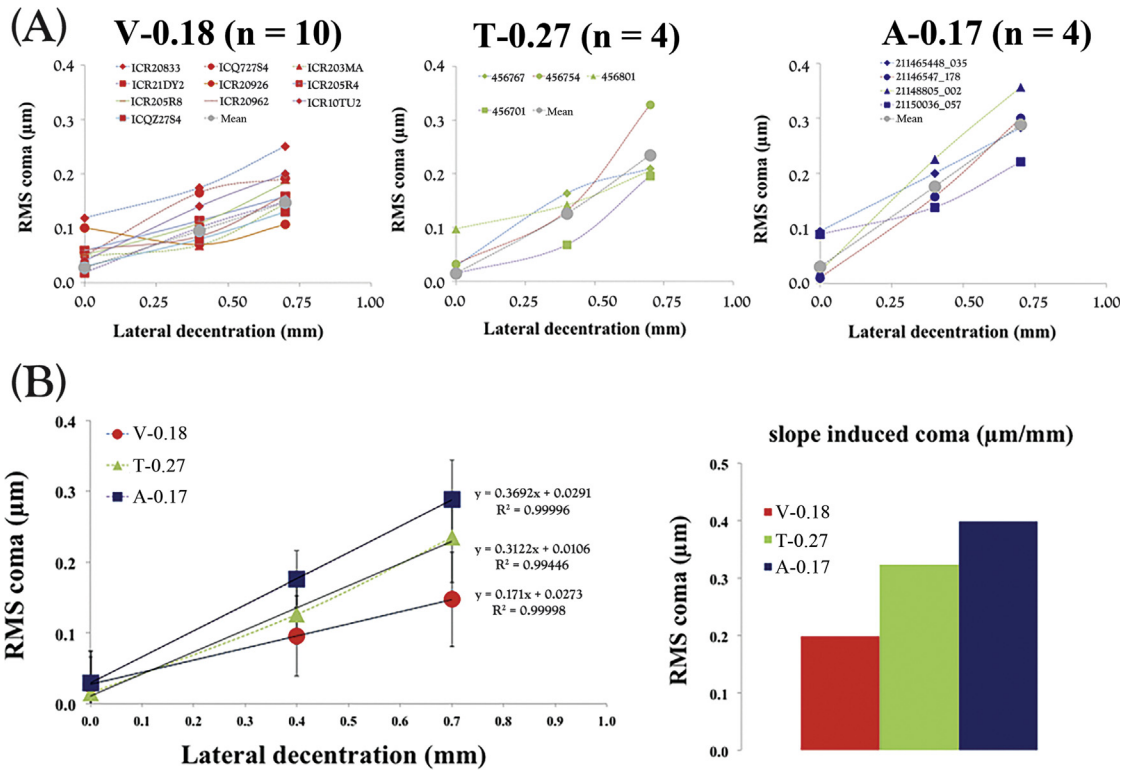

Figure 2. *A*: Root-mean-square coma versus decentration by intraocular lens model. *B*: Root-mean-square coma versus decentration (mean). Data are for a 4.0 mm pupil diameter (RMS = root mean square).

calculations were made) for V-0.18 IOL, T-0.27 IOL, and A-0.17 IOL, respectively. Figure 3, *C*, shows the visual Strehl ratio for green (at best focus) relative to red (defocused by the chromatic difference of focus) for centered IOLs and for IOLs decentered by 0.4 mm and 0.7 mm. The impact of chromatic defocus depended on the IOL material and decreased with increasing decentration.

DISCUSSION

We evaluated the effect of IOL decentration on retinal image quality by experimentally measuring wave aberrations in physical eye models containing different aspheric IOLs. Although the results were in good agreement with predictions using computer eye models (based on cornea-measured and IOL-measured geometry), the aberrometric measurements allowed us to evaluate the influence of real factors (including the manufacturing variability of IOL geometry). To our knowledge, this is the first report of monochromatic aberrations and optical quality as function of IOL decentration with different IOL models and a large sample size (18 IOL samples). All tested IOL models (Vivinex XY1 [V-0.17], Tecnis 1P ZCB00V [T-0.27], and Acrysof 1P SN60WF [A-0.17]) have aspheric surfaces and are designed to correct (to some extent) the spherical aberration of the average cornea. However, decentration of different IOL models has a different effect on aberration (in particular astigmatism and coma) and therefore on optical quality.

We found the V-0.18 IOL to be the most immune to decentration. According to its manufacturer, this is the result of technology that modulates the optical surfaces (disclosed in the patent[17]), also known as the aspheric balance curve, which is intended to balance coma aberrations. In practice, in the central optical area, this IOL has 2 aspheric zones

Table 2. Results of astigmatism and coma with 4 randomly selected V-0.18 IOLs.

	Mean ± SD					
	Astigmatism (D)			Coma (µm)		
Test	On Axis	0.4 mm	0.7 mm	On Axis	0.4 mm	0.7 mm
10 IOLs	0.05 ± 0.01	0.09 ± 0.03	0.15 ± 0.03	0.03 ± 0.03	0.10 ± 0.06	0.15 ± 0.06
4 IOLs (#1)	0.04 ± 0.01	0.08 ± 0.02	0.14 ± 0.02	0.02 ± 0.01	0.08 ± 0.02	0.14 ± 0.02
4 IOLs (#2)	0.05 ± 0.01	0.07 ± 0.02	0.15 ± 0.04	0.04 ± 0.04	0.12 ± 0.05	0.18 ± 0.05
4 IOLs (#3)	0.04 ± 0.01	0.09 ± 0.03	0.16 ± 0.04	0.06 ± 0.03	0.12 ± 0.05	0.19 ± 0.05
4 IOLs (#4)	0.05 ± 0.01	0.11 ± 0.02	0.16 ± 0.03	0.05 ± 0.03	0.10 ± 0.03	0.16 ± 0.04

IOLs = intraocular lenses

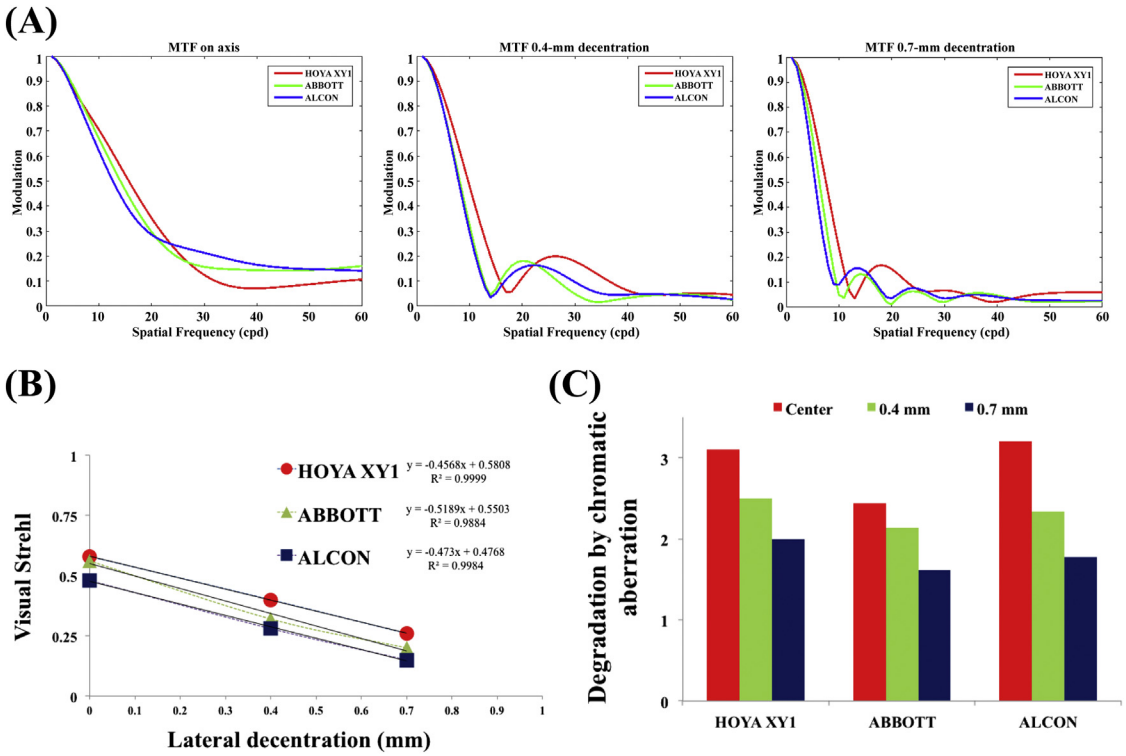

Figure 3. *A*: The MTF of the physical model eye with all measured IOLs. Data are for a 4.0 mm pupil diameter. *B*: Visual Strehl values of the physical model eye with all measured IOLs. *C*: Effect of chromatic defocus (relative data) (cpd = cycles per degree; IOLs = intraocular lenses; MTF = modulation transfer function).

designed to decrease the impact of misalignment between the IOL and the visual axis (decentration) on the quality of vision. This idea is to sustain the optical image quality through a wider range of misalignment better than conventional aspheric optical designs. Connection between spherical aberration and coma and the possibility of balancing coma by modulation of aspheric IOL designs are recognized in the classic Seidel aberration theory.[26] Barbero et al.[6] reported isoplanatic aspheric IOL designs that improved off-axis optical quality (ie, by reducing coma and astigmatism) over standard designs using 4th-order aspheric surfaces and a multi-configuration approach to optimize image quality at various angles. Tabernero et al.[27] found that the shape factor of an IOL influenced the correction of coma.

We also found that the presence of chromatic defocus attenuated the impact of IOL decentration and that conversely, the presence of decentration decreased the degradation of chromatic defocus. This finding is in agreement with results in previous studies[21,24,25] that showed HOAs and chromatic aberration interacted positively, suggesting a defensive role of aberrations against chromatic blur.

Although in general there are marked and significant differences in optical performance and its change with IOL decentration across IOL designs, larger differences were found across IOL samples of the same design (eg, the SD for the radius of curvature of the anterior IOL surface varied from 0.47 mm in the T-0.27 IOL to 2.06 mm in A-0.17 IOL) than across repeated measurements on the same sample; for example, the SD (5 repeated measurements) for the radius of curvature for 1 V-0.18 IOL was 0.07 mm. Part of the inter-sample variability might be associated with slight differences in resulting IOL geometry in the manufacturing process, as shown by metrology measurements (based on noncontact profilometry) of the IOL surfaces. We found mean RMS differences of 0.19 μm, 0.33 μm, and 0.34 μm in the anterior IOL surface and 0.59 μm, 0.46 μm, 0.51 μm in the posterior IOL surface of the V-0.18 IOL, T-0.27 IOL, and A-0.17 IOL, respectively, which is consistent with previously published ex vivo metrology variability.[28] These individual differences might be associated with the reproducibility in the polishing stage during the manufacturing process. Also, some differences in measurements might result from the mounting process. For example, consistent residual astigmatism in a centered IOL (in particular with the A-0.17) might be associated with tension in the haptic attachment in the IOL holder of the physical model eye. Nevertheless, the rate of change of astigmatism or coma did not appear affected by this.

The study evaluated 2 decentration magnitudes (0.0 mm and 0.7 mm). The relative decrease in optical quality with decentration in the physical model eye, which was close to diffraction limited for a centered IOL (visual Strehl ratio, 0.5 to 0.6) appears to be higher than that found in real eyes. At 0.7 mm of lateral decentration, the visual Strehl ratio decreased by 55% in the V-0.18 IOL, 64% in the T-0.27 IOL, and 68% in A-0.17 IOL. The typical IOL decentration in real eyes is reported to range between 0.14 mm and

0.46 mm.[19,20] In fact, in a study by Rosales and Marcos,[2] some decentration improved optical quality over that with a centered IOL a large proportion (60%) of eyes. The presence of other HOAs in real eyes, in particular the additional presence of IOL tilt and foveal misalignment, attenuate the impact of decentration and might produce favorable interactions with appropriate amounts and orientation of decentration.

In summary, laser ray-tracing measurements allowed us to evaluate the individual robustness of different IOL designs against imperfect IOL alignment and the relative contribution of decentration to the retinal image quality, including astigmatism and HOAs. Of the 3 tested IOLs, the Vivinex XY1 was the most immune to optical degradation caused by decentration. Further in vivo studies of a population with different corneal aberrometry profiles would provide insight into the robustness of different IOL designs against decentration.

WHAT WAS KNOWN

- In general, state-of-the-art aspheric monofocal IOLs reduce positive spherical aberration of the cornea.
- Increasing the number of surface design parameters confers better control for reducing astigmatism or coma. However, it has been argued that as IOL designs become more complex, final intraocular positioning becomes more critical.

WHAT THIS PAPER ADDS

- Intraocular lens design has a clear impact on the induction of astigmatism and coma when the IOL is decentered, with some designs being less immune to optical degradation when decentered.

REFERENCES

1. Atchison DA. Design of aspheric intraocular lenses. Ophthalmic Physiol Opt 1991; 11:137–146
2. Rosales P, Marcos S. Customized computer models of eyes with intraocular lenses. Opt Express 2007; 15:2204–2218. Available at: https://www.osapublishing.org/DirectPDFAccess/09B6AD96-AE9A-AB22-6CBA9925552021F9_130575/oe-15-5-2204.pdf?da=1&id=130575&seq=0&mobile=no. Accessed March 27, 2018
3. Barbero S, Marcos S. Analytical tools for customized design of monofocal intraocular lenses. Opt Express 2007; 15:8576–8591. Available at: http://digital.csic.es/bitstream/10261/8575/3/Analytical_tools.pdf. Accessed March 27, 2018
4. Einighammer J, Oltrup T, Feudner E, Bende T, Jean B. Customized aspheric intraocular lenses calculated with real ray tracing. J Cataract Refract Surg 2009; 35:1984–1994
5. Tabernero J, Piers P, Benito A, Redondo M, Artal P. Predicting the optical performance of eyes implanted with IOLs to correct spherical aberration. Invest Ophthalmol Vis Sci 2006; 47:4651–4658. Available at: http://iovs.arvojournals.org/article.aspx?articleid=2124955. Accessed March 27, 2018
6. Barbero S, Marcos S, Montejo J, Dorronsoro C. Design of isoplanatic aspheric monofocal intraocular lenses. Opt Express 2011; 19:6215–6230. Available at: https://www.osapublishing.org/DirectPDFAccess/0A0CF34B-EE6D-E46F-3D37D569A916DBFC_210901/oe-19-7-6215.pdf?da=1&id=210901&seq=0&mobile=no. Accessed March 27, 2018
7. Taketani F, Matsuura T, Yukawa E, Hara Y. Influence of intraocular lens tilt and decentration on wavefront aberrations. J Cataract Refract Surg 2004; 30:2158–2162
8. McKelvie J, McArdle B, McGhee C. The influence of tilt, decentration, and pupil size on the higher-order aberration profile of aspheric intraocular lenses. Ophthalmology 2011; 118:1724–1731
9. Marcos S, Barbero S, Jiménez-Alfaro I. Optical quality and depth-of-field of eyes implanted with spherical and aspheric intraocular lenses. J Refract Surg 2005; 21:223–235
10. Rosales P, De Castro A, Jiménez-Alfaro I, Marcos S. Intraocular lens alignment from Purkinje and Scheimpflug imaging. Clin Exp Optom 2010; 93:400–408. Available at: http://onlinelibrary.wiley.com/doi/10.1111/j.1444-0938.2010.00514.x/epdf. Accessed March 27, 2018
11. Eppig T, Scholz K, Löffler A, Meßner A, Langenbucher A. Effect of decentration and tilt on the image quality of aspheric intraocular lens designs in a model eye. J Cataract Refract Surg 2009; 35:1091–1100
12. Baumeister M, Bühren J, Kohnen T. Tilt and decentration of spherical and aspheric intraocular lenses: effect on higher-order aberrations. J Cataract Refract Surg 2009; 35:1006–1012
13. Altmann GE, Nichamin LD, Lane SS, Pepose JS. Optical performance of 3 intraocular lens designs in the presence of decentration. J Cataract Refract Surg 2005; 331:574–585
14. Marcos S, Ortiz S, Pérez-Merino P, Birkenfeld J, Durán S, Jiménez-Alfaro I. Three-dimensional evaluation of accommodating intraocular lens shift and alignment in vivo. Ophthalmology 2014; 121:45–55. Available at: http://www.aaojournal.org/article/S0161-6420(13)00529-0/pdf. Accessed March 27, 2018
15. Rosales P, Marcos S. Pentacam Scheimpflug quantitative imaging of the crystalline lens and intraocular lens. J Refract Surg 2009; 25:421–428
16. Marcos S, Rosales P, Llorente L, Barbero S, Jiménez-Alfaro I. Balance of corneal horizontal coma by internal optics in eyes with intraocular artificial lenses: evidence of a passive mechanism. Vision Res 2008; 48:70–79
17. Sanger D, Lawu T, inventors; Hoya Corporation, assignee. Intraocular lens. U.S. Patent US 8,647,383 B2, February 11, 2014. Available at: https://patentimages.storage.googleapis.com/8d/1a/11/d987403a54448c/US8647383.pdf. Accessed March 27, 2018
18. Ortiz C, Esteve-Taboada JJ, Belda-Salmerón L, Monsálvez-Romín D, Domínguez-Vicent A. Effect of decentration on the optical quality of two intraocular lenses. Optom Vis Sci 2016; 93:1552–1559. Available at: https://journals.lww.com/optvissci/Fulltext/2016/12000/Effect_of_Decentration_on_the_Optical_Quality_of.14.aspx. Accessed March 27, 2018
19. de Castro A, Rosales P, Marcos S. Tilt and decentration of intraocular lenses in vivo from Purkinje and Scheimpflug imaging; validation study. J Cataract Refract Surg 2007; 33:418–429
20. Ortiz S, Pérez-Merino P, Durán S, Velasco-Ocana M, Birkenfeld J, de Castro A, Jiménez-Alfaro I, Marcos S. Full OCT anterior segment biometry: an application in cataract surgery. Biomed Opt Express 2013; 4:387–396. Available at: http://www.ncbi.nlm.nih.gov/pmc/articles/PMC3595049/pdf/387.pdf. Accessed March 27, 2018
21. Pérez-Merino P, Dorronsoro C, Llorente L, Durán S, Jiménez-Alfaro I, Marcos S. In vivo chromatic aberration in eyes implanted with intraocular lenses. Invest Ophthalmol Vis Sci 2013; 54:2654–2661. Available at: http://iovs.arvojournals.org/article.aspx?articleid=2189112. Accessed March 27, 2018
22. Tandogan T, Son HS, Choi CY, Knorz MC, Auffarth GU, Khoramnia R. Laboratory evaluation of the influence decentration and pupil size on the optical performance of a monofocal, bifocal, and trifocal intraocular lens. J Refract Surg 2017; 33:808–812
23. Pérez-Merino P, Ortiz S, Alejandre N, de Castro A, Jiménez-Alfaro I, Marcos S. Ocular and optical coherence tomography-based corneal aberrometry in keratoconic eyes treated by intracorneal ring segments. Am J Ophthalmol 2014; 157:116–127
24. Nakajima M, Hiraoka T, Yamamoto T, Takagi S, Hirohara Y, Oshika T, Mihashi T. Differences of longitudinal chromatic aberration (LCA) between eyes with intraocular lenses from different manufacturers. PLoS One 2016; 11(6):e0156227. Available at: https://www.ncbi.nlm.nih.gov/pmc/articles/PMC4892582/pdf/pone.0156227.pdf. Accessed March 27, 2018
25. McLellan JS, Marcos S, Prieto PM, Burns SA. Imperfect optics may be the eye's defense against chromatic blur [letter]. Nature 2002; 417:174–176. Available at: http://www.opt.indiana.edu/people/faculty/burns/pub/McLellan_211_Final.pdf. Accessed March 27, 2018
26. Fincham WHA, Freeman MH. Optics, 9th ed. Boston, MA, Butterworths, 1980; section 18.6, second line in equation 18.37

27. Tabernero J, Piers P, Artal P. Intraocular lens to correct corneal coma. Opt Lett 2007; 32:406–408. Available at: https://lo.um.es/panel/secciones/noticias/adjuntos/58.pdf. Accessed March 27, 2018
28. Sheehan MT. Eye Modelling for Personalised Intraocular Lens Design [dissertation]. Galway, Ireland, National University of Ireland, 2012. Available at: https://aran.library.nuigalway.ie/bitstream/handle/10379/3020/2012sheehanphd.pdf?sequence=1&isAllowed=y. Accessed March 27, 2018

Disclosures: *None of the authors has a financial or proprietary interest in any material or method mentioned.*